IMPROVED MODELLING OF WAVE-CURRENT INTERACTION IN SWAN

André van der Westhuysen[1]

Recent hindcast studies in the Amelander Zeegat tidal inlet in the Dutch Wadden Sea have shown the significant influence of currents on the prediction of wave fields by the spectral wave model SWAN. In following current, observations are typically well reproduced, but under strong opposing current, wave heights are significantly overestimated. Ris and Holthuijsen (1996) propose that such overestimations are due to insufficient steepness dissipation of waves on an opposing current gradient. The present paper presents a new formulation for the enhanced dissipation of waves on a counter current gradient which is scaled with the degree of Doppler shifting, and hence steepness increase, due to the current. This expression contains one additional unknown parameter, which is calibrated using laboratory observations. This formulation is suitable for both mature wave fields and young wind sea conditions. Application of this enhanced dissipation term to a data set of Amelander Zeegat field cases shows an improvement for opposing current situations in the tidal channel. For following current, no significant deterioration of results is found. In particular, the results for the young wind sea on the tidal flats are not significantly affected, unlike with the Ris and Holthuijsen (1996) expression.

Keywords: wave-current interaction; wave dissipation; SWAN

1. INTRODUCTION

The Dutch Wadden Sea (Fig. 1) is a complex coastal system that poses significant challenges to nearshore wave modelling. The region is enclosed by a series of barrier islands and the mainland coasts of the provinces of Friesland and Groningen. Tidal inlets are found between the barrier islands, each featuring an ebb tidal delta, one or more main tidal channels, and a complex system of smaller channels and flats extending into the Wadden Sea interior. Apart from the tidal channels, the Wadden Sea interior is shallow and flat, with tidally-modulated depths normally ranging between 0 m (dry fall) and 3 m. Recent hindcast studies with the spectral wave model SWAN (Booij et al. 1999) conducted in the Amelander Zeegat (Groeneweg et al. 2008; Van Vledder et al. 2008) have shown the significant influence of currents on the prediction of wave fields in the tidal inlets. In following current, observations are typically well reproduced, but under opposing current with strong gradients, wave heights are significantly overestimated. This affects the reliability with which these predictions can be applied in the assessment of safety from flooding. This issue is addressed in the present study.

Ris and Holthuijsen (1996), hereafter RH96, show that SWAN, using the whitecapping expression of Komen et al. (1984), underestimates wave dissipation in opposing current gradients, leading to a strong overestimation of significant wave heights. This agrees with the model behaviour found in the Amelander Zeegat. Models for enhanced wave dissipation in adverse current gradients have been proposed by RH96, Chawla and Kirby (1998, 2002) and Suastika and Battjes (2009). These authors all assume a bore-based breaker model (either Battjes and Janssen (1978) or Thornton and Guza (1983)), with the mean wave steepness as governing parameter, to be appropriate for modelling the current-induced dissipation. However, Chawla and Kirby (1998) note from experimental observations that current-induced breaking is very different from depth-induced breaking - the breaking is weak and unsaturated, as opposed to the saturated breakers observed in depth-induced breaking. As a practical problem, Ris (1997) reports that the model of RH96 fails under wind-wave growth situations, since young wind waves, being inherently steep, are too strongly dissipated. This approach is therefore unsuitable for field situations that feature a combination of wind growth and current interaction, like the Dutch Wadden Sea. Hence, an alternative approach is necessary for the dissipation of waves on counter current gradients.

In this study, a formulation for the dissipation of waves on adverse current gradients is presented that is suitable for both mature wave fields and young wind sea conditions. It is calibrated and validated for a range of laboratory and field situations.

The enhanced dissipation of waves on counter current gradients is modelled here by means of a saturation-based expression for the whitecapping dissipation. Here the expression of Alves and Banner (2003), as adapted by Van der Westhuysen et al. (2007), is applied. It will be shown that the proposed calibration settings for this expression, obtained for wind wave growth conditions, yield too

---
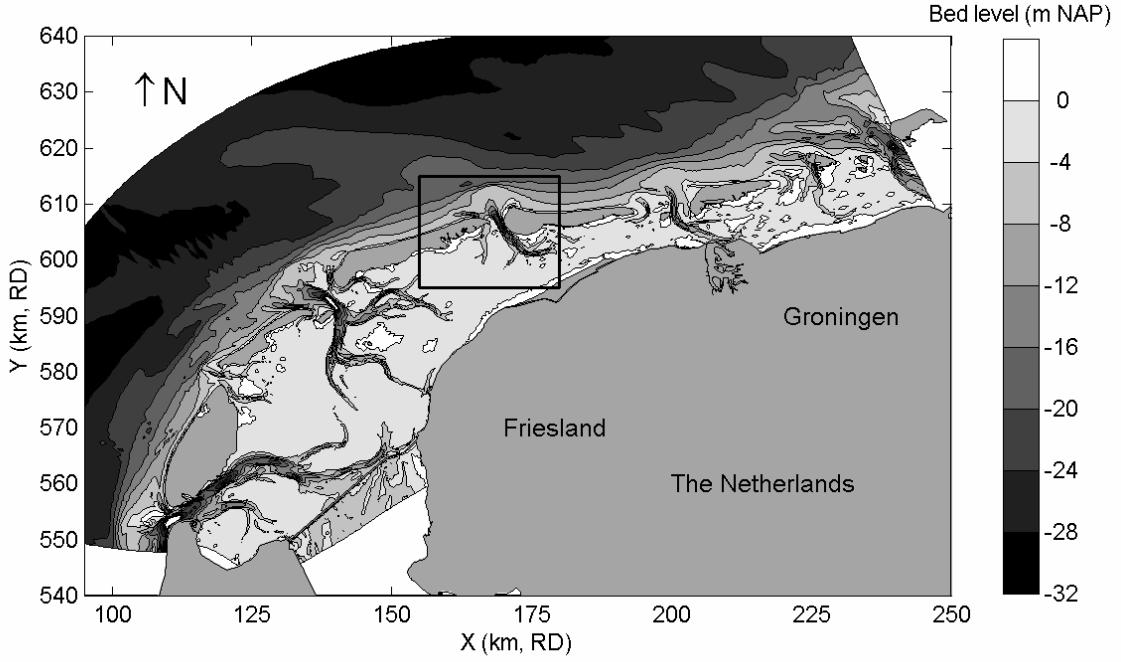
Figure 1. Bathymetry of the Dutch Wadden Sea in the north of the Netherlands, with the Amelander Zeegat indicated. Coordinates in the Dutch RD system and bed levels relative to the leveling datum NAP.

little dissipation on opposing current gradients (as was found for the Komen et al. (1984) expression by RH96). It is conversely not desirable to recalibrate the whitecapping expression for application to current-induced dissipation, as suggested by Chawla and Kirby (2002), as this will be at the expense of predictions for wind wave growth. Hence, in this study the saturation-based expression is combined with a scaling that enhances dissipation proportional to the degree of steepening of waves by the gradient in the opposing current. The latter process is isolated by considering the effect of current-induced Doppler shifting on the wave steepness.

This paper is structured as follows: Section 2 presents the methodology followed in this study, including the models applied and the case selection. In Section 3, the proposed enhanced dissipation formulation is calibrated and in Section 4 it is validated. Section 5 closes the paper with conclusions.

2. METHOD

This section presents the methodology of this study. This includes an overview of the action balance equation in SWAN and the additions proposed here (Section 2.1), details of these formulations for enhanced current-induced dissipation (Section 2.2), the model settings applied (Section 2.3), the selection of cases for the calibration and validation of the proposed formulations (Section 2.4).

2.1 Additions to the action balance equation

The spectral model SWAN computes the evolution of wave action density N (= E/σ, where E is the variance density and σ the relative radian frequency) using the action balance equation:

$$\frac{\partial N}{\partial t} + \nabla_{x,y} \cdot \left[\left(\vec{c}_g + \vec{U} \right) N \right] + \frac{\partial}{\partial \theta} \left(c_\theta N \right) + \frac{\partial}{\partial \sigma} \left(c_\sigma N \right) = \frac{S_{tot}}{\sigma} \tag{1}$$

and

$$S_{tot} = S_{in} + S_{wc} + S_{nl4} + S_{bot} + S_{brk} + S_{nl3} \left(+ S_{wc,cur} \right) \tag{2}$$

The terms on the left-hand side of Eq. 1 represent, respectively, the change of wave action in time, the propagation of wave action in geographical space (with $\vec{c}_g$ the linear wave group velocity vector and $\vec{U}$ the ambient current), depth- and current-induced refraction (with propagation velocity c_θ in directional space θ) and the shifting of the relative radian frequency σ due to variations in mean current and depth (with the propagation velocity c_σ). The right-hand side of Eq. 1 represents processes that generate, dissipate or redistribute wave energy, given by Eq. 2. In deep water, three source terms are traditionally used: the transfer of energy from the wind to the waves, S_{in}; the dissipation of wave energy due to whitecapping, S_{wc}; and the nonlinear transfer of wave energy due to quadruplet (four-wave) interaction, S_{nl4}. In shallow water, dissipation due to bottom friction, S_{bot}, depth-induced breaking, S_{brk}, and nonlinear triad (three-wave) interaction, S_{nl3}, are additionally accounted for. In the present study, an additional source term is included in Eq. 2, namely a term for the enhanced breaking dissipation of waves on a current, $S_{wc,cur}$.

2.2 Models for enhanced breaking dissipation on counter current

Below, various formulations for steepness breaking (whitecapping) are presented. Firstly, the saturation-based whitecapping expression proposed by Van der Westhuysen (2007) is presented. Subsequently, two formulations for enhanced breaking dissipation on counter current are described, namely the expression of RH96 and the formulation proposed in the present study.

Default saturation-based whitecapping

Van der Westhuysen (2007) proposes a saturation-based whitecapping expression that is an adapted version of the formulation developed by Alves and Banner (2003). This expression is combined with the wind input formulation proposed by Yan (1987). The whitecapping expression of Van der Westhuysen (2007) is composed of two parts, namely a contribution to the dissipation by wave breaking, and a weaker non-breaking contribution:

$$S_{wc}(\sigma,\theta) = f_{br}(\sigma) S_{dis,break} + \left[1 - f_{br}(\sigma)\right] S_{dis,non-break} \qquad (3)$$

where

$$S_{dis,break}(\sigma,\theta) = -C_{ds}\left[\frac{B(k)}{B_r}\right]^{p/2} \left[\tanh(kd)\right]^{\frac{2-p}{4}} g^{\frac{1}{2}} k^{\frac{1}{2}} E(\sigma,\theta) \qquad (4)$$

and

$$S_{dis,non-break}(\sigma,\theta) = -C'_{ds}\left(\frac{k}{\tilde{k}}\right)^q \left(\frac{\tilde{s}}{\tilde{s}_{PM}}\right)^r \tilde{\sigma} E(\sigma,\theta) \qquad (5)$$

in which f_{br} is a weighting factor determining the changeover from the dissipation of breaking to non-breaking waves. This weighting is a function of the ratio between the spectral saturation $B(k)$ and a threshold saturation level B_r:

$$f_{br}(\sigma) = \frac{1}{2} + \frac{1}{2}\tanh\left\langle 10\left(\left[\frac{B(k)}{B_r}\right]^{1/2} - 1\right)\right\rangle \qquad (6)$$

Eq. 4 is based on the saturation-based expression of Alves and Banner (2003), as described in Van der Westhuysen et al. (2007), and Eq. 5 on the pulse-based expression of Komen et al. (1984). For the spatial scales considered in the field cases of the present study, only the component in Eq. 4 is relevant. The parameter p is a function of the inverse wave age u_*/c, based on scaling arguments involving a spectral balance between the wind input, whitecapping and nonlinear interaction terms:

$$p\left(u_*/c\right) = 3 + \tanh\left[25\left(\frac{u_*}{c} - 0.1\right)\right] \tag{7}$$

In Van der Westhuysen (2007), the parameters of Eq. 4 were calibrated to $C_{ds} = 5.0 \times 10^{-5}$ and $B_r = 1.75 \times 10^{-3}$ respectively.

Ris and Holthuijsen (1996)

As discussed in Section 1, RH96 show that the default pulse-based whitecapping expression of Komen et al. (1984) does not provide sufficient wave breaking dissipation in situations of strong opposing current gradients. They demonstrate that the addition of a dissipation term based on the bore-based breaker model of Battjes and Janssen (1978) to Eq. 2 is effective in the modelling of the rapid dissipation occurring near the blocking point. This expression reads:

$$S_{wc,cur}\left(\sigma,\theta\right) = -C''_{ds}Q_b\left(\frac{s_{max}}{\tilde{s}}\right)^2 \tilde{\sigma}\frac{k}{\tilde{k}}E\left(\sigma,\theta\right) \tag{8}$$

where $\tilde{s}$ is the mean wave steepness, $\tilde{\sigma}$ the mean relative radian frequency and $\tilde{k}$ the mean wave number, defined as

$$\tilde{k} = \left(E_{tot}^{-1}\int_0^{2\pi}\int_0^{\infty}\frac{1}{\sqrt{k}}E\left(\sigma,\theta\right)d\sigma d\theta\right)^{-2} \tag{9}$$

The proportionality coefficient $C''_{ds} = \alpha_{BJ} = 1$. The variable Q_b is the fraction of breaking waves, computed as

$$\frac{1-Q_b}{\ln Q_b} = -8\frac{E_{tot}}{H_m^2} \tag{10}$$

in which a maximum wave height H_m is defined based on a limiting steepness

$$H_m = \frac{2\pi s_{max}}{\tilde{k}} \tag{11}$$

The limiting steepness s_{max} is set to 0.14, based on Miche's criterion for the limiting steepness of an individual breaker. We note that Chawla and Kirby (1998) show that when propagating on a counter current, waves can break at a lower steepness than this. RH96 demonstrate that Eq. 8 enhances the dissipation for waves exceeding a mean steepness of $\tilde{s} = 0.08$, such as can occur in strong adverse currents.

Enhanced saturation-based dissipation

In Section 1 it was argued from observational evidence that a bore-based approach is not the most suitable for modelling current-induced wave breaking, and that a dependence on mean wave steepness can be problematic in field situations that include inherently steep young wind sea. It is therefore proposed that the form of the saturation-based whitecapping expression Eq. 4 be applied to model the enhanced dissipation term $S_{wc,cur}$ in Eq. 2. In order to isolate the contribution of currents in the increased steepness and resulting dissipation, the degree of enhanced dissipation by Eq. 4 is scaled with the normalised propagation speed of the relative radian frequency in frequency space, given by c_{σ}/σ. Dimensional analysis then yields:

$$S'_{wc,cur} = -C''_{ds} \max\left[\frac{c_\sigma(\sigma,\theta)}{\sigma}, 0\right]\left[\frac{B(k)}{B_r}\right]^{p/2} E(\sigma,\theta) \qquad (12)$$

where the propagation speed c_σ is given by (e.g. Whitham 1974):

$$c_\sigma = \frac{d\sigma}{dt} = \frac{\partial\sigma}{\partial d}\left[\frac{\partial d}{\partial t} + \vec{U}\cdot\nabla_{x,y}d\right] - c_g\vec{k}\cdot\frac{\partial\vec{U}}{\partial r} \quad, \qquad (13)$$

in which d is the water depth and r the space coordinate in the wave propagation direction. In the present study, the focus is on the changes in c_σ due to gradients in the current. For simplicity, the shallow water scaling factor $\left[\tanh(kd)\right]^{\frac{2-p}{4}}$ in Eq. 4, found by Van der Westhuysen et al. (2007) to have relatively little effect, has been dropped in Eq. 12. A maximum function is included in order to take only relative increases in steepness into account in the enhanced dissipation. Note that this can also occur for negative gradients in following current, although overall dissipation levels would typically be lower. The parameterizations of B_r and p are taken similar to those of Eq. 4. Hence, Eq. 12 contains one additional calibration parameter relative to Eq. 4, namely the proportionality coefficient C''_{ds}. Its calibration is considered in Section 3.

2.3 Model settings

The computations presented here were performed using the SWAN model version 40.72ABC, in stationary third-generation mode. For the deep water physics, the combination of wind input S_{in} and saturation-based whitecapping S_{wc} proposed by Van der Westhuysen (2007) was applied. Quadruplet nonlinear interaction S_{nl4} was modelled using the Discrete Interaction Approximation (DIA) of Hasselmann et al. (1985). The shallow water source terms include triad nonlinear interaction S_{nl3} according to Eldeberky (1996) and bottom friction according to Hasselmann et al. (1973), both with their default settings in SWAN. For depth-induced breaking S_{brk}, the biphase breaker model of Van der Westhuysen (2010) was applied, with the extension proposed by Van der Westhuysen (2009). Hereafter, these settings will be referred to as the default model. Two further variants are studied, featuring the additional expressions for enhanced current-induced dissipation presented above. The curvature-based convergence criteria of Zijlema and Van der Westhuysen (2005) are applied.

2.4 Data sets

In order to assess the performance of the proposed expression for wave dissipation on counter current, a data set of laboratory and field cases has been assembled, which is presented below.

Lai et al. (1989) flume experiment

Lai et al. (1989) investigated the transformation of the wave spectrum under strong adverse currents in a flume 8 m in length and 0.75 m in depth. A current flow was induced along the flume, which was contracted by the presence of a shoal, resulting in an increase in the current velocity from U = -0.13 to -0.22 m/s over the shoal. Waves were mechanically generated at the downstream end of the flume. In the case considered here, the incident wave field had a significant wave height of H_{m0} = 0.019 m and a mean period of T_{m01} = 0.5 s. This resulted in a partially blocking situation with U/c_g = 0.52 at the spectral peak. The observed significant wave height decreases strongly over the shoal due to partial blocking by the counter current. At the same time, the observed absolute mean wave period increases going over the shoal. This increase in the mean period is due to the blocking of wave components with absolute frequencies higher than approximately 2 Hz.

Suastika et al. (2000) flume experiment

Suastika et al. (2000) and Suastika and Battjes (2009) studied partial and full wave blocking using a 35 m long flume, with a 12 m measurement section at its centre. Three of these cases are considered here, all involving partial blocking with U/c_g = 0.47 at the spectral peak. Waves were mechanically generated at the one end of the flume. A water head difference induced current flow along the flume, running in the up-wave direction. At the measurement section, the flow was con-
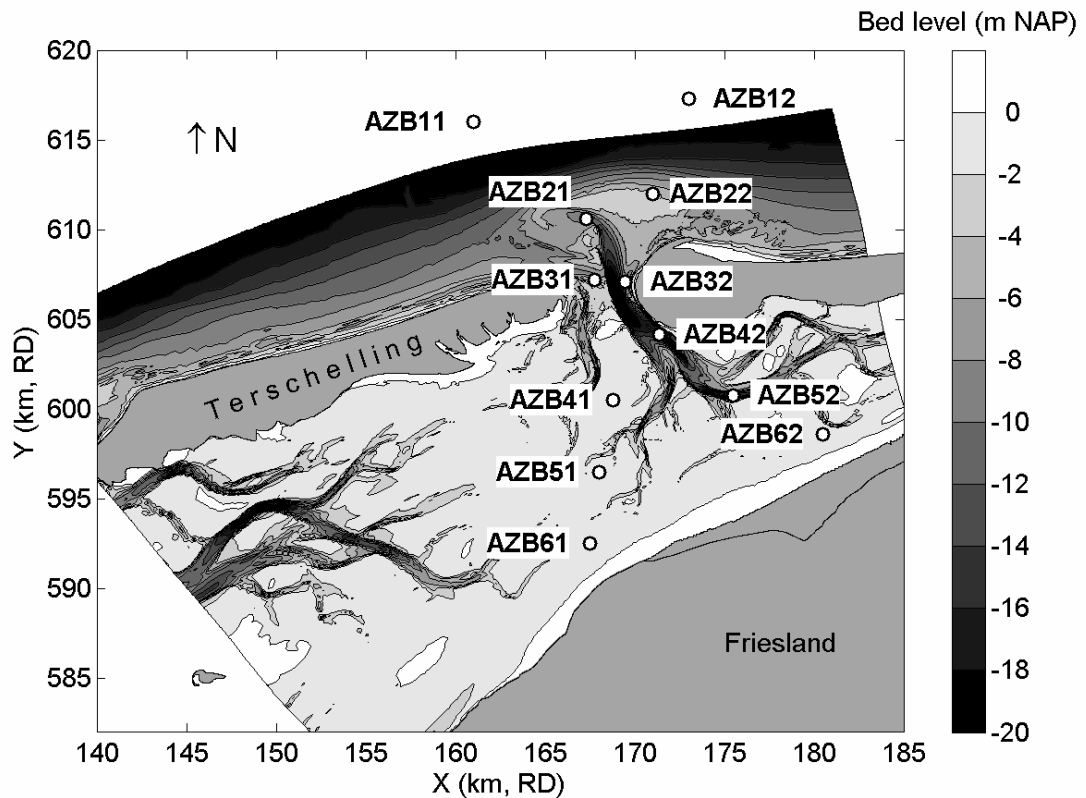
Figure 2. Bathymetry of the Amelander Zeegat, including the location of wave measurement buoys. Coordinates in the Dutch RD system and bed levels relative to the leveling datum NAP.

tracted by an inner flume wall and bottom. The discharge entering at the upstream (down-wave) end was gradually withdrawn through the bottom of the inner flume by pumps, creating a counter-current that reduced approximately linearly to zero in the up-wave direction. The perforated bottom of this inner flume allowed withdrawal of discharge into the adjacent outer half of the flume, which acted as a sump for the suction pumps. However, the presence of this false bottom had the disadvantage of introducing an additional source of dissipation, which was accounted for using an empirical percolation dissipation term (see Suastika 2004; Suastika and Battjes 2009). A further term for dissipation due to side wall friction proposed by these authors was not included here.

Amelander Zeegat

Conditions in the Dutch Wadden Sea are represented by a collection of 27 stationary cases taken from NW and W storms occurring over the Amelander Zeegat (Fig. 2) during 2007. The NW storms feature high water levels (up to 2.6 m NAP) combined with high winds of 11.8 to 18.5 m/s from predominantly 320-331°N, whereas the W storms feature equally high winds of 11.9 to 20.3 m/s from 264-279°N. During the NW events, the wind and offshore waves were directed more or less straight into the tidal channel. Although during W events the wind direction was not parallel to the tidal channel, offshore waves turn and propagate into the tidal channel by refraction over the ebb tidal delta. During these events, two arrays of wave buoys were placed along transects through the tidal inlet, making them well-situated to record conditions of wave-current interaction. Current information, which was not observed, was computed using the hydrodynamic model Delft3D.

3. CALIBRATION

The expression for enhanced dissipation Eq. 12 features one calibration parameter, namely the proportionality coefficient C''_{ds}, the calibration of which is considered next. The laboratory flume cases of Lai et al. (1989) and Suastika et al. (2000) were used for this purpose. Fig. 3 presents the cali-
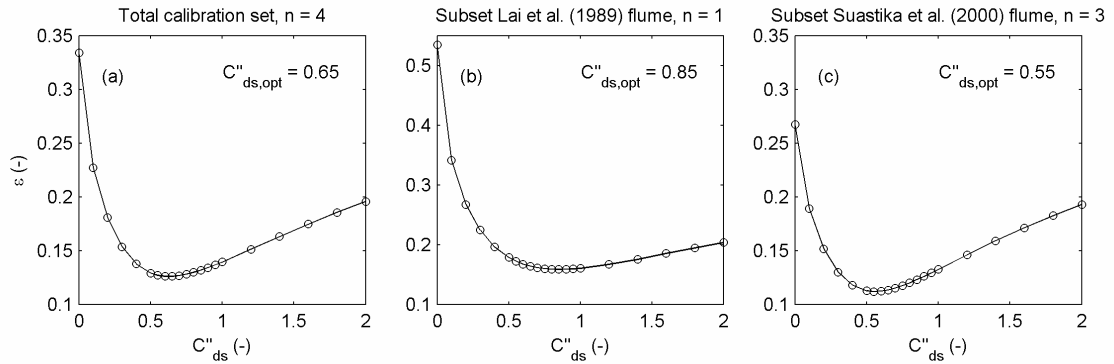
Figure 3. Calibration of Eq. 12. Error function ε as a function of proportionality coefficient C''_{ds} for various calibration subsets. Number of cases in each set denoted by n.
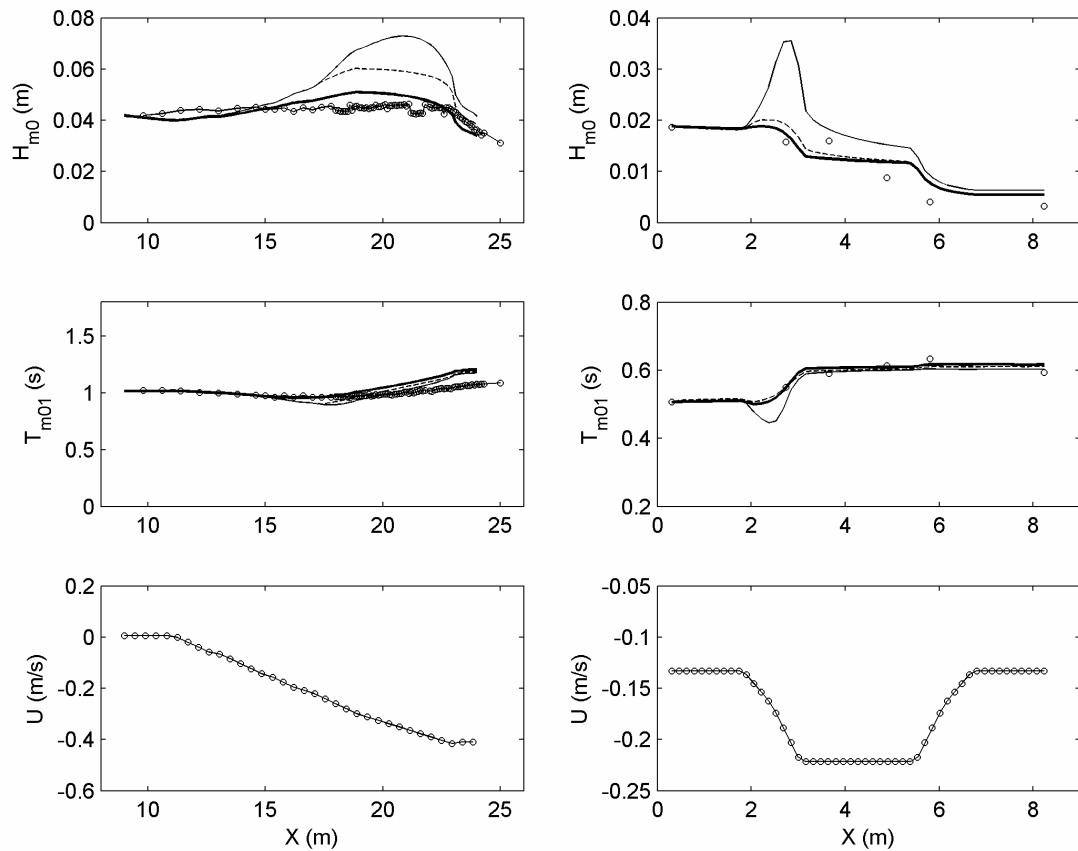
Figure 4. Calibration results for Eq. 12. Comparison between the default (solid), RH96 (dashed) and proposed models with C''_{ds} = 0.65 (thick solid). Observations given by circles. Left-hand panels: flume experiment by Suastika et al. (2000). Right-hand panels: Lai et al. (1989).

bration of C''_{ds} by means of optimalisation of the error function $\varepsilon = \frac{1}{2}\left(SI_H + SI_T\right)$, where SI_H and SI_T are the scatter indexes of H_{m0} and $T_{m-1,0}$ respectively. Fig. 3 presents the variation of this error function with C''_{ds} for the total calibration data set, and for each of the two subsets it is composed of. Panels (b) and (c) both show that the error ε has a (local) maximum at a value of $C''_{ds} = 0$ in the individual calibration subsets, indicating the importance of including the dissipation term Eq. 12. The data sets furthermore display a relatively high sensitivity to the coefficient C''_{ds} in the range $0 < C''_{ds} < 0.5$, demonstrating the impact of applying Eq. 12. The calibration result for the total calibration data set (panel (a)) gives an optimal setting of $C''_{ds} = 0.65$.

Fig. 4 presents the calibration results in terms of spatial evolution for two of the above cases, with the results for the RH96 expression included for comparison. The left-hand panels of Fig. 4 show the calibration results (with $C''_{ds} = 0.65$) for a partial blocking case of Suastika et al. (2000). A significant improvement in the significant wave height over that of both the default and RH96 models is found. The mean wave period is predicted less accurately, however, showing an overestimation going towards the partial blocking region. Inspection of the frequency spectra reveals that this is due to an overestimation of the frequency downshift of spectral components in SWAN (not shown). For the flume case of Lai et al. (1989), the strong overestimation of the significant wave height and the underestimation of the mean period with the default model are corrected using Eq. 12 (Fig. 4, right-hand panels). This improvement is similar to that found with the RH96 expression.

The default version of SWAN applies the linear dispersion relation in the propagation part of Eq. 1. Since Chawla and Kirby (2002) report an influence of nonlinear dispersion in wave blocking situations, the sensitivity of the present results to the application of Stokes third-order dispersion was investigated. It was found that for the present partial blocking flume cases, the addition of nonlinear dispersion in the default model moved the partial blocking region further upstream, but that the strong overestimation of H_{m0} along the flume remains (not shown). Nonlinear dispersion could therefore not explain the observed overestimations, and was therefore omitted in the remainder of the study.

4. VALIDATION

Having calibrated Eq. 12, its performance is evaluated on the basis of the validation data set of NW and W storms recorded in the Amelander Zeegat inlet during 2007, and compared with the performance of the RH96 expression. The conditions in these cases are equally distributed between opposing and following current in the inlet, with a number of opposing current cases exceeding 1 m/s. Scaled with the wave group velocity, maximum opposing relative current speeds of around $U/c_g = 0.4$ are found, which are still relatively far from the blocking point. In addition to the settings given in Section 2.3, the modelling of these cases also feature the process of diffraction, which is modelled here using the phase-decoupled expression of Holthuijsen et al. (2003).

Fig. 5 compares model results with observations in terms of scatter plots of H_{m0}, $T_{m-1,0}$ and the non-dimensional ratio H_{m0}/d. These parameters have been computed over the frequency range 0.03-0.5 Hz. The left-hand column shows the results of the default model, featuring the whitecapping expression of Van der Westhuysen (2007) without enhanced whitecappping. Although the general agreement between the model results and the observations is good, the wave heights in the tidal channel (buoys AZB32/42/52, indicated with filled symbols, with statistics in parentheses) is overestimated by an average of 9%. For conditions with counter current, this is related to insufficient dissipation of waves steepening in counter current gradients, as illustrated by the flume cases above. The results for the mean period and the H_{m0}/d ratio show good agreement with the observations, with a slight negative bias in higher values of H_{m0}/d (middle and bottom left-hand panels).

The centre column of Figure 5 presents the simulation results of the default model with the addition of the RH96 expression. With this additional term, the overestimation of the significant wave height at the buoys AZB32/42/52 in the channel is reduced to 4%. However, the integral parameters at the buoys in the shallow interior (AZB41/51/61/62) are now structurally underpredicted. This is seen, for example, in the underprediction of the higher values of H_{m0}/d associated with this region (bottom panels). For these buoys, inherently steep, young wind sea is excessively dissipated by RH96. As a result, the overall statistics of this model variant are poorer than those of the default model.

The right-hand column of Fig. 5 presents the corresponding results for the default model in combination with the enhanced dissipation Eq. 12, using the calibrated value $C''_{ds} = 0.65$. The general performance of the model can be seen to be similar to that of the default model, although with some
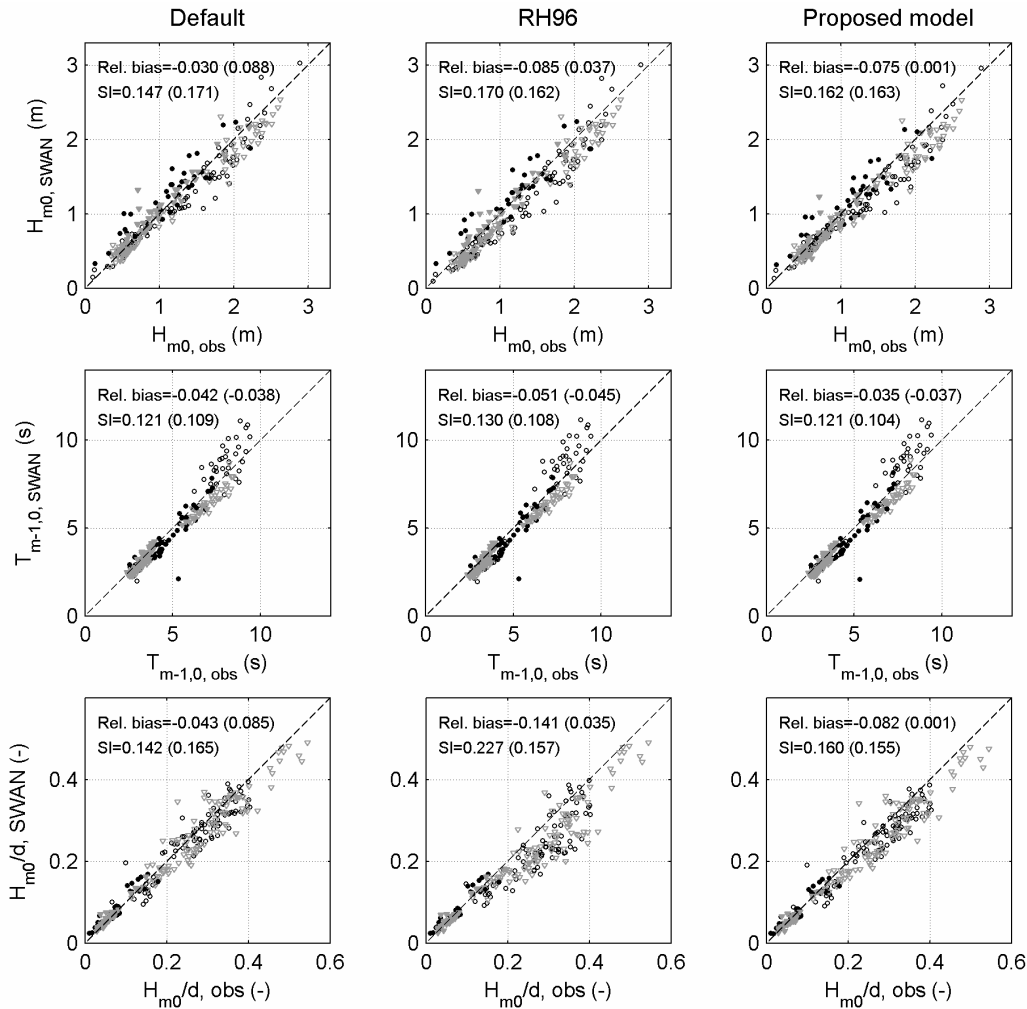
Figure 5. Scatter plot results of the default and proposed models for the January/March 2007 (inverted triangles) and November 2007 (circles) Amelander Zeegat validation cases. Filled symbols denote stations in the tidal channel, with statistics in parentheses.

deterioration of the overall statistical scores. However, for the channel buoys AZB32/42/52 the 9% overestimation in H_{m0} found with the default model is now corrected (top panels). The improvement is the most pronounced for the cases of the November 2007 storm, for which a number of data points were overestimated using the default model. For the January/March 2007 storms, similar, although less pronounced improvement in predicted significant wave heights is found. However, importantly, application of Eq. 12 does not significantly deteriorate the model results of the younger wind sea over the tidal flats, as is the case with the RH96 expression (compare bottom panels showing H_{m0}/d ratio). The overall error statistics of H_{m0} and H_{m0}/d now show a greater negative bias due to the correction of the overestimated wave heights at the channel buoys. This result suggests the need for further development or recalibration of the remaining source terms, now including the current-induced dissipation term in Eq. 2. Finally, Fig. 5 shows that the results for the absolute mean period $T_{m-1,0}$ are rather insensitive to the application of Eq. 12, with only a slight reduction in the overall bias.

Figures 6 and 7 present examples of the frequency spectra (in terms of absolute frequency) at the wave buoys AZB42 and AZB61 in the Amelander Zeegat (see Fig. 2) produced by the three model variants. Fig. 6 shows three cases for which the buoy AZB42 in the tidal channel is subjected to opposing ebb current. At this buoy, the default model can be seen to overestimate the wind sea growth, with an overestimation of both the total variance and the peak frequency. Application of the enhanced dissipation expression of RH96 yields some improvement at the buoy location AZB42, but still over-
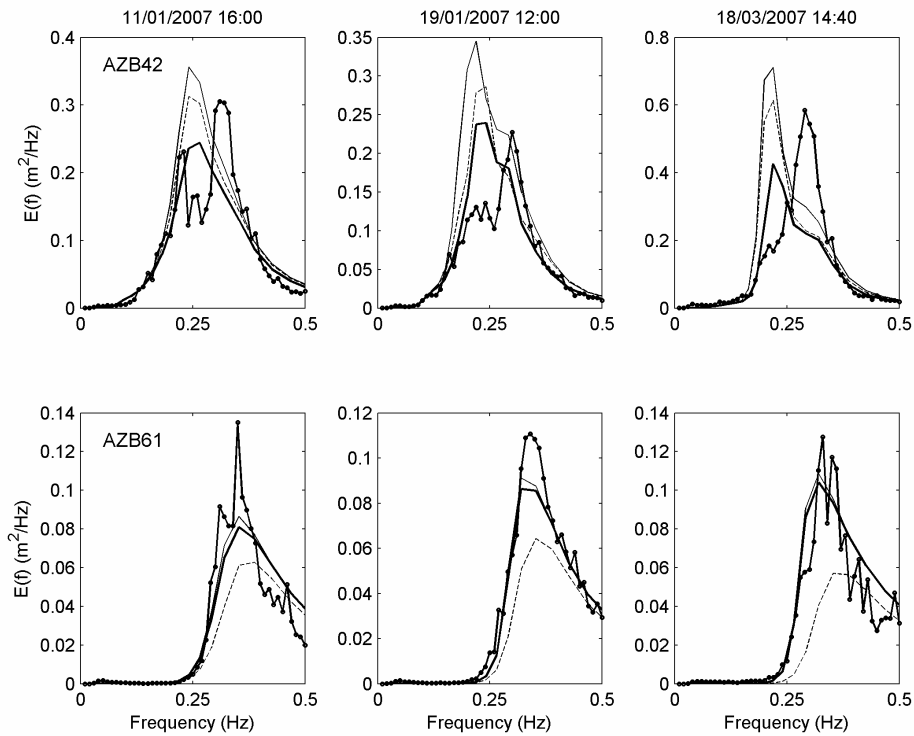
Figure 6. Absolute frequency spectra produced by the default (solid), RH96 (dashed) and proposed (thick solid) models for various ebb cases in the Amelander Zeegat in 2007. Observations denoted by line with circles.
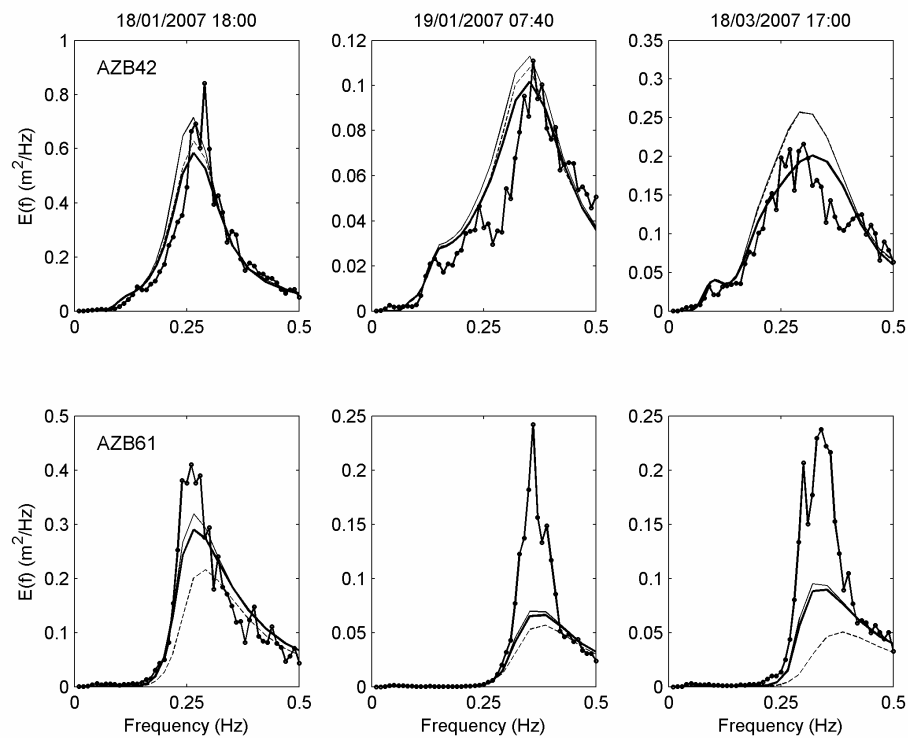
Figure 7. As in Fig. 6, but for various flood cases in the Amelander Zeegat in 2007.

estimates the observations. By contrast, at the buoy AZB61, located on the tidal flats, the RH96 model significantly underestimates the growth of the young wind sea, as was seen in the scatter plots in Fig. 5 above. The model run featuring the enhanced whitecapping expression of Eq. 12 yields a better prediction at AZB42 in the tidal channel than either the default or the RH96 variants, although the position of the peak frequency is still not predicted well. However, unlike with the RH96 expression, the results at AZB61 are mostly unaffected, as desired.

Fig. 7 presents examples of frequency spectra for various flood situations in the Amelander Zeegat. For these cases, the default model reproduces the observed spectra fairly well. Since waves are elongated under the influence of a positive gradient in the following current, they are not expected to become steeper and break, and hence the enhanced whitecapping dissipation considered here is not expected to have any effect. Indeed, at the buoy location AZB42, the model results have only a small sensitivity to the application of either the RH96 or the proposed dissipation expressions, as desired. An exception is found for the case 18/03/2007 at 17:00. Here a number of spectral directions experience opposing current gradients, and hence are dissipated by Eq. 12, resulting in lower spectral densities at AZB42 than with the default model. As seen above, the RH96 expression yields strong underestimations at the buoy AZB61 on the tidal flats. By contrast, the model variant featuring the enhanced dissipation Eq. 12 has only a limited impact on the results at this location. It should be noted, however, that in some cases neither the default model, nor the proposed variant manages to correctly predict the peak spectral densities at AZB61. Correction of these inaccuracies is considered to be beyond the scope of the present study.

5. CONCLUSIONS

The objective of the present study was to correct the overestimation of wave heights on opposing current gradients in SWAN, as found in the tidal channels of the Wadden Sea. The model inaccuracy was addressed by the development of a formulation for the enhanced breaking dissipation of waves that is related to the degree of their current-induced steepening. This formulation was calibrated and validated for a range of laboratory and field situations. The following conclusions can be drawn from the results of this study:

1. Using a diverse set of laboratory and field cases, the results of this study confirm that the default SWAN model overestimates significant wave heights in the presence of opposing current gradients, as found earlier by Ris and Holthuijsen (1996). Experimental observations of wave breaking near the blocking point suggest that this model inaccuracy is due to an insufficient degree of steepness dissipation (whitecapping) under these conditions.
2. The results of this study confirm that the addition of enhanced whitecapping dissipation according to Ris and Holthuijsen (1996) improves results for laboratory cases. However, as shown by Ris (1997), this expression leads to underestimation of young wind sea due to its inherent high steepness. This results in significant underestimation of locally-generated wind sea over the tidal flats in the Wadden Sea interior.
3. A new formulation for the enhanced dissipation of waves on counter current is proposed which is based on the saturation-based formulation of Van der Westhuysen et al. (2007), and scaled with the degree of Doppler shifting per spectral component, which is related to the current-induced steepening of the wave field. This expression contains one additional unknown parameter, which was calibrated to a value of $C''_{ds} = 0.65$ using laboratory and field observations.
4. Validation of the proposed enhanced dissipation term for a data set of Amelander Zeegat field cases shows that the overestimation of significant wave heights at the channel buoys under opposing current is corrected. The satisfactory prediction of the mean period $T_{m-1,0}$ is retained. For situations with following current, no significant deterioration of results is found. In particular, the results for the locally-generated wind sea on the tidal flats are not significantly affected, unlike with the expression of Ris and Holthuijsen (1996).

REFERENCES

Alves, J.H.G.M., Banner, M.L. 2003. Performance of a saturation-based dissipation-rate source term in modelling the fetch-limited evolution of wind waves. *J. of Phys. Oceanogr.*, 33, 1274-1298.

Battjes, J.A., and J.P.F.M. Janssen. 1978. Energy loss and set-up due to breaking of random waves, *Proceedings of 14th International Conference on Coastal Engineering*, ASCE, 466-480.

Booij, N., R.C. Ris and L.H. Holthuijsen. 1999. A third generation wave model for coastal regions, Part I, Model description and validation, *J. Geophys. Res.*, 104, C4, 7649-7666.

Chawla, A. and J.T. Kirby. 1998. Experimental study of wave breaking and blocking on opposing currents, *Proc. 26th Int. Conf. Coastal Eng.*, ASCE, 759-772.

Chawla, A. and J.T. Kirby. 2002. Monochromatic and random wave breaking at blocking points, *J. Geophys. Res.*, 107(C7), 10.1029/2001JC001042.

Eldeberky, Y. 1996. Nonlinear transformations of wave spectra in the nearshore zone, *Ph.D Thesis*, Fac. of Civil Engineering, Delft University of Technology, 203 pp.

Groeneweg, J., A.J. van der Westhuysen, G.P. van Vledder, S. Jacobse, J. Lansen and A.R. van Dongeren. 2008. Wave modelling in a tidal inlet: Performance of SWAN in the Wadden Sea, *Proc. 31th Int. Conf. Coastal Eng.*, ASCE, 411-423.

Hasselmann, K., T.P. Barnett, E. Bouws, H. Carlson, D.E. Cartwright, K. Enke, J.A. Ewing, H. Gienapp, D.E. Hasselmann, P. Kruseman, A. Meerburg, O. Müller, D.J. Olbers, K. Richter, W. Sell, and H. Walden. 1973. Measurement of wind-wave growth and swell decay during the Joint North Sea Wave Project (JONSWAP), *Dtsch. Hydrogr. Z. Suppl., A(8)*, 12, 95 pp.

Hasselmann, S., K. Hasselmann, J.A. Allender, and T.P. Barnett. 1985. Computations and parameterizations of the nonlinear energy transfer in a gravity-wave spectrum. Part 2: parameterization of the nonlinear transfer for application in wave models, *J. of Phys. Oceanogr.* 15, 1378-1391.

Holthuijsen, L.H., A. Herman and N. Booij. 2003. Phase-decoupled refraction-diffraction for spectral wave models, Coastal Eng., 49, 291-305.

Komen, G. J., S. Hasselmann, and K. Hasselmann. 1984. On the existance of a fully developed wind-sea spectrum, *J. of Phys. Oceanogr.* 14, 1271-1285.

Lai, R.J., S.R. Long and N.E. Huang. 1989. Laboratory studies of wave-current interaction: Kinematics of the strong interaction, *J. Geophys. Res.*, 94, 16,201-16,214.

Ris, R.C. 1997. Spectral modelling of wind waves in coastal waters, *Ph.D Thesis*, Fac. Of Civil Eng., Delft Univ. of Tech., 160pp.

Ris, R.C., and L.H. Holthuijsen. 1996. Spectral modelling of current wave-blocking. *Proc. 25th Int. Conf. on Coastal Eng.*, ASCE, 1247-1254.

Suastika, I.K. 2004. Wave blocking, *Ph.D Thesis*, Fac. Of Civil Eng., Delft Univ. of Tech., 157pp.

Suastika, I.K. and J.A. Battjes. 2009. A model for blocking of periodic waves. *Coastal Eng. J.*, 51(2), 81-99.

Suastika, I.K., M.P.C. de Jong and J.A. Battjes. 2000. Experimental study of wave blocking. *Proc. 27th Int. Conf. Coastal Eng.*, ASCE, 227-240.

Thornton, E.B., and R.T. Guza. 1983. Transformation of wave height distribution, *J. Geophys. Res.* 88, 5925-5938.

Van der Westhuysen, A.J. 2007. Advances in the spectral modelling of wind waves in the nearshore, *Ph.D Thesis*, Fac. of Civil Engineering, Delft University of Technology, 207pp.

Van der Westhuysen, A.J. 2009. Modelling of depth-induced wave breaking over sloping and horizontal beds. *Proc. 11th Int. Workshop on Wave Hindcasting and Forecasting and Coastal Hazard Symposium*, JCOMM Technical Report 52, WMO/TD-No. 1533.

Van der Westhuysen, A.J. 2010. Modeling of depth-induced wave breaking under finite-depth wave growth conditions. *J. Geophys. Res*, 115, C01008, doi:10.1029/2009JC005433.

Van der Westhuysen, A.J., M. Zijlema, and J.A. Battjes. 2007. Nonlinear saturation-based whitecapping dissipation in SWAN for deep and shallow water, *Coastal Eng.*, 54, 151-170.

Van Vledder, G.P., J. Groeneweg and A.J. van der Westhuysen. 2008. Numerical and physical aspects of wave modelling in a tidal inlet, *Proc. 31th Int. Conf. Coastal Eng.*, ASCE, 424-436.

Whitham, G.B. 1974. *Linear and nonlinear waves*, John Wiley, New York, 636 pp.

Yan, L. 1987. An improved wind input source term for third generation ocean wave modelling. *Technical Report No. 87-8, Royal Dutch Meteor. Inst. (KNMI).*

Zijlema, M., and A.J. van der Westhuysen. 2005. On convergence behaviour and numerical accuracy in stationary SWAN simulations of nearshore wind wave spectra, *Coastal Eng.*, 52, 237-256.